Applying $\mathbf{W}$ on $\vec{u}$ then gives

$$\mathbf{W}\,\vec{u} \;=\; \sum_{i=1}^{n} a_i\,\lambda_i\,\vec{u}_i\;, \tag{10.25}$$

and doing so k consecutive times gives

$$\mathbf{W}^k\,\vec{u} \;=\; \sum_{i=1}^{n} a_i\,\lambda_i^k\,\vec{u}_i \;=\; \lambda_1^k\left[a_1\vec{u}_1 \;+\; \sum_{i=2}^{n} a_i\,(\lambda_i/\lambda_1)^k\,\vec{u}_i\right]\;. \tag{10.26}$$

Since $|\lambda_i/\lambda_1| < 1$ for $i \neq 1$, all but the first term in the square brackets will decrease in magnitude relative to the first term as $k \to \infty$. Thus, for large k we eventually get

$$\mathbf{W}^k\,\vec{u} \;\approx\; a_1\lambda_1^k\vec{u}_1\;, \tag{10.27}$$

and hence $\vec{u}_1$ can be obtained by normalizing $\mathbf{W}^k\,\vec{u}$.

While this method targets the dominant eigenvalue, there are various extensions which are able to find states other than the one with the largest eigenvalue. For example, if we know that there is an upper bound Λ for the magnitudes of the eigenvalues, we can apply the power method to the modified (and shifted) matrix $\Lambda^2\mathbf{I} - \mathbf{W}^2$ and obtain the eigenstate with the eigenvalue of the smallest magnitude (say, the ground state wave function). Alternatively, we can also consider the application of the power method with $\mathbf{W}^{-1}$ if we are interested in the ground state. It turns out that this can be accomplished without actually inverting the matrix first. Similarly, it is possible to use the combinations of shifting and inversion to look for eigenstates with eigenvalues in a neighborhood of values of our choice. Moreover, once an eigenstate and its eigenvalue are obtained by such a method, it is possible to iteratively project out the linear space associated with such states and look for the next most dominant one, and so forth. We will not dwell any further on this method, but it can be a very effective way to obtain a specific state, such as the one with the largest (or the smallest) eigenvalue.

10.4 A VARIATIONAL APPROACH

The computational difficulties with a "direct" matrix approach to eigenvalue problems have motivated the development of a number of alternative schemes. We do not have space to discuss all of them here; the interested reader can explore some of them through the references. In this section we will introduce one of these schemes to give an example of how the Schrödinger equation can be attacked. The method we now describe involves a Monte Carlo approach, similar to that described in Chapter 8, coupled with the variational principle.

The variational principle of quantum mechanics can be expressed as follows. Let φ be a "trial" wave function. We imagine that we are searching for the ground-state solution to the Schrödinger equation for a particular problem and that φ is a proposed wave function, or perhaps our best numerical guess for the true wave function. We can calculate the "energy" corresponding to this trial function

$$E^* \;\equiv\; \frac{\int \varphi^*\,\mathcal{H}\,\varphi\,d\vec{r}}{\int \varphi^*\,\varphi\,d\vec{r}}\;, \tag{10.28}$$

where the integrations are over all space and $\mathcal{H}$ is the Hamiltonian operator. Note that we have given this effective energy the symbol E^* to emphasize the fact that since φ is not necessarily a solution of (10.17) (it was only a "proposed" wave function), E^* is not necessarily the energy of a true eigenstate.

According to the variational principle, the true ground-state energy is *always* less than or equal to E^*. In fact, the only time they are equal is when the trial wave function is precisely the true ground-state wave function. For *all* other functions φ the effective energy E^* will be higher than the ground-state energy. This principle allows us to recast the problem of solving the Schrödinger equation as a minimization problem. The goal is to find the function φ which minimizes E^*. There are several ways to implement this strategy, corresponding to different ways of searching through the space of all possible wave functions. The approach we describe below is very general, yet also somewhat crude. After seeing how it works, we will consider improved ways of constructing φ and performing the search procedure, some of which will be explored in the exercises.

To be specific we consider again the problem of finding the ground state of the one-dimensional Lennard-Jones potential. We dealt with this problem earlier with the matching method, so we already have a solution with which to compare it. To implement a minimization strategy we must first choose an initial trial wave function, which we will call φ^0. As usual, we discretize space into bins Δx in size and let φ_n^0 be the value of the initial trial function at $x = n\Delta x$. We also restrict the domain[25] of our function to the range $x = 0.7 - 5$ (in reduced units), since we know on physical grounds that the ground state will be one in which the particle is localized near the minimum in the potential, $x_{\min} \sim 1.1$. Hence, our bins run from $n = 0$ corresponding to $x = 0.7$, up to $n = N$ corresponding to $x = 5$. We choose an extremely simple initial trial function: $\varphi_n^0 =$ constant for $1 \leq x \leq 4$ and zero outside this range, as shown in Figure 10.14. The constant is determined by requiring that our function satisfy the normalization condition $\int \varphi^* \varphi \, dx = 1$. This is certainly a poor approximation to the true ground-state wave function, so if the method can succeed with this choice of φ^0 it can probably be successful with any choice!

The only remaining part of the algorithm that must be specified is the procedure for how to use φ^0 (or any other trial function) to obtain an improved trial function. We will employ a Monte Carlo approach, which operates as follows. First, we pick one of the bins along x at random by choosing an integer in the range 0–N; we will call this bin *ntest*. Second, we construct a provisional function by changing the value of the trial function at that location, φ^0_{ntest}, by an amount chosen randomly in the range $\pm d\varphi$. Third, we calculate E^* for this provisional function. If it is lower than the corresponding value for φ^0, the provisional function must be "closer" to the true wave function, and we use it as the new trial function. If E^* for the provisional function is higher than the value for φ^0, we discard the provisional function and keep φ^0 as the trial function.[26]

[25] We will take $\sigma = 1$ and $\epsilon = 10$ in (10.12), so that the potential is the same as that considered in Figure 10.8.

[26] Unlike the Monte Carlo method employed in Chapter 8, the algorithm described here does not involve a temperature parameter to enable changes that increase the energy. However, it

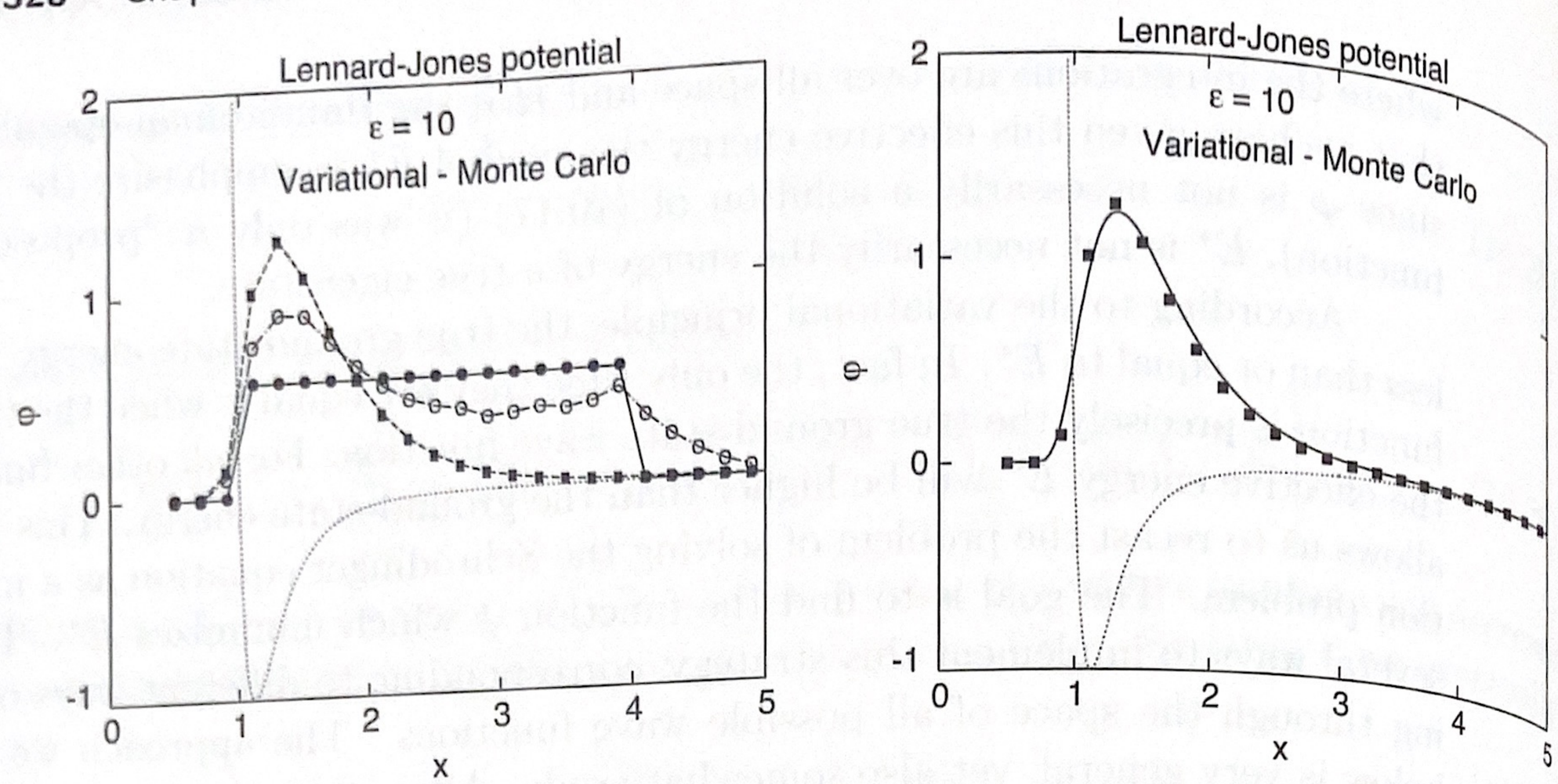

FIGURE 10.14: Left: trial wave functions, φ, during the course of a variational–Monte Carlo calculation for the Lennard-Jones problem. The filled circles show the initial trial function, φ^0, the open circles show the trial function after 10^3 attempted Monte Carlo moves (i.e., changes in the wave function), and the squares show it after 10^4 attempted moves. E^* for these trial wave functions was 0.11, -1.43, and -2.18, respectively. Right: comparison of the final variational wave function with the results of the matching method (Figure 10.8). The filled squares here are the best trial functions from the plot on the left. Note that both of these wave functions have been properly normalized and that the potential (the dotted curves) is not shown to scale.

We will leave the construction of a variational–Monte Carlo program to the exercises (a full listing of such a program is given at this book's Web site). All of the key ingredients of such a program have been described above. We will mention only one programming subtlety here. You must decide at the outset whether or not the trial functions are to be properly normalized (and if so, when to do it). This arises when evaluating E^*, since if φ is normalized the denominator in (10.28) is unity and thus need not be computed. For this reason it is convenient to always normalize φ. However, if you perform this normalization after each tentative Monte Carlo modification of the trial function, you must make sure that you can return to the previous trial function if the Monte Carlo modification is rejected.

As the Monte Carlo process is repeated many times, both the trial function and the corresponding value of E^* should converge to those of the true ground state. Some results for the trial function for the Lennard-Jones problem at various stages of the calculation are shown on the left in Figure 10.14. After a relatively small number of Monte Carlo iterations (10^3 in Figure 10.14), φ exhibits fluctuations that arise because this function was constructed from a small collection of random changes. However, after a large number of Monte Carlo adjustments φ becomes a smooth function of x, as we would expect for the true wave function. The final trial

---

is often useful to allow such energy increases with some probability *temporarily*, reducing such probability gradually as the procedure goes forward and the energy approaches the ground state energy. This is called *simulated annealing* and is described in Appendix B. Strictly prohibiting energy increases would correspond to quenching the system instantly to zero temperature, while simulated annealing corresponds to a more gradual decrease in temperature.

function shown here had an energy $E^* = -2.18$, which agrees with the value found with the matching method (Figure 10.8) to within about 10 percent. The trial function itself also agrees well with the wave function calculated with the matching method, as shown on the right in Figure 10.14. There are some slight differences and we will show in the exercises that they are due to the finite grid size used in describing the variational wave function.

The variational–Monte Carlo method can thus deal effectively with one dimensional situations such as the Lennard-Jones problem. However, its real strength is that it can be applied with very little additional effort to treat two- and three-dimensional cases. To illustrate this we now consider a particle confined by a two-dimensional harmonic potential. The Schrödinger equation in this case is (10.1) with the potential

$$V(x,y) = \frac{1}{2}\, k_x\, x^2 + \frac{1}{2}\, k_y\, y^2 \,, \tag{10.29}$$

where k_x and k_y are related to the curvatures of the potential in the x and y directions. The astute reader will notice that this problem can be separated into two independent one-dimensional harmonic oscillators, one along x and one along y, which can be solved analytically. We will use this exact solution to evaluate the usefulness of the variational–Monte Carlo method. Several problems for which there are no known exact analytic solutions will be considered in the exercises.

To implement the variational approach for the two-dimensional oscillator we discretize space along the x and y directions into segments of length Δx and Δy, and write our trial functions as $\varphi(m,n)$, with $x = m\Delta x$, and $y = n\Delta x$ (for convenience we take $\Delta y = \Delta x$). We also restrict x and y to the range $-N\Delta x \le x \le N\Delta x$ and $-N\Delta x \le y \le N\Delta x$, so that we have $(2N+1)^2$ bins altogether. For this calculation we again pick an extremely simple initial trial wave function, $\varphi^0 =$ constant for all points in the region $|x| \le 1.6$ and $|y| \le 1.6$, and zero otherwise. This trial function is shown in Figure 10.15.

The Monte Carlo algorithm can then be implemented as in our previous example. During each Monte Carlo step a grid location (mtest, ntest) is chosen at random, and a provisional function obtained by changing the initial trial function φ^0(mtest, ntest) by a small amount chosen randomly from the range $\pm d\varphi$. If E^* for this provisional function is lower than that of φ^0, then the provisional function becomes the new trial wave function. If E^* is higher, we keep φ^0 as the trial function. Some results are given in Figure 10.15, where on the left we show the trial function as the calculation proceeds. The final trial function has a roughly Gaussian shape, which may be familiar to you from the analytic solution of the harmonic oscillator. Figure 10.15 also shows the behavior of E^* during the calculation. It is a monotonically decreasing function, as required by the Monte Carlo procedure. After many Monte Carlo time steps it approaches a constant, which signals the convergence of the algorithm.

A plot of the final trial wave function as a function of both x and y is shown in Figure 10.16. The wave function falls off more slowly in the x direction than along y, since in this example we have chosen $k_x < k_y$. This means that the "spring constant" for vibrations along x was softer than the one along y, so the effective amplitude of vibration was larger along x. The value of E^* for this trial function

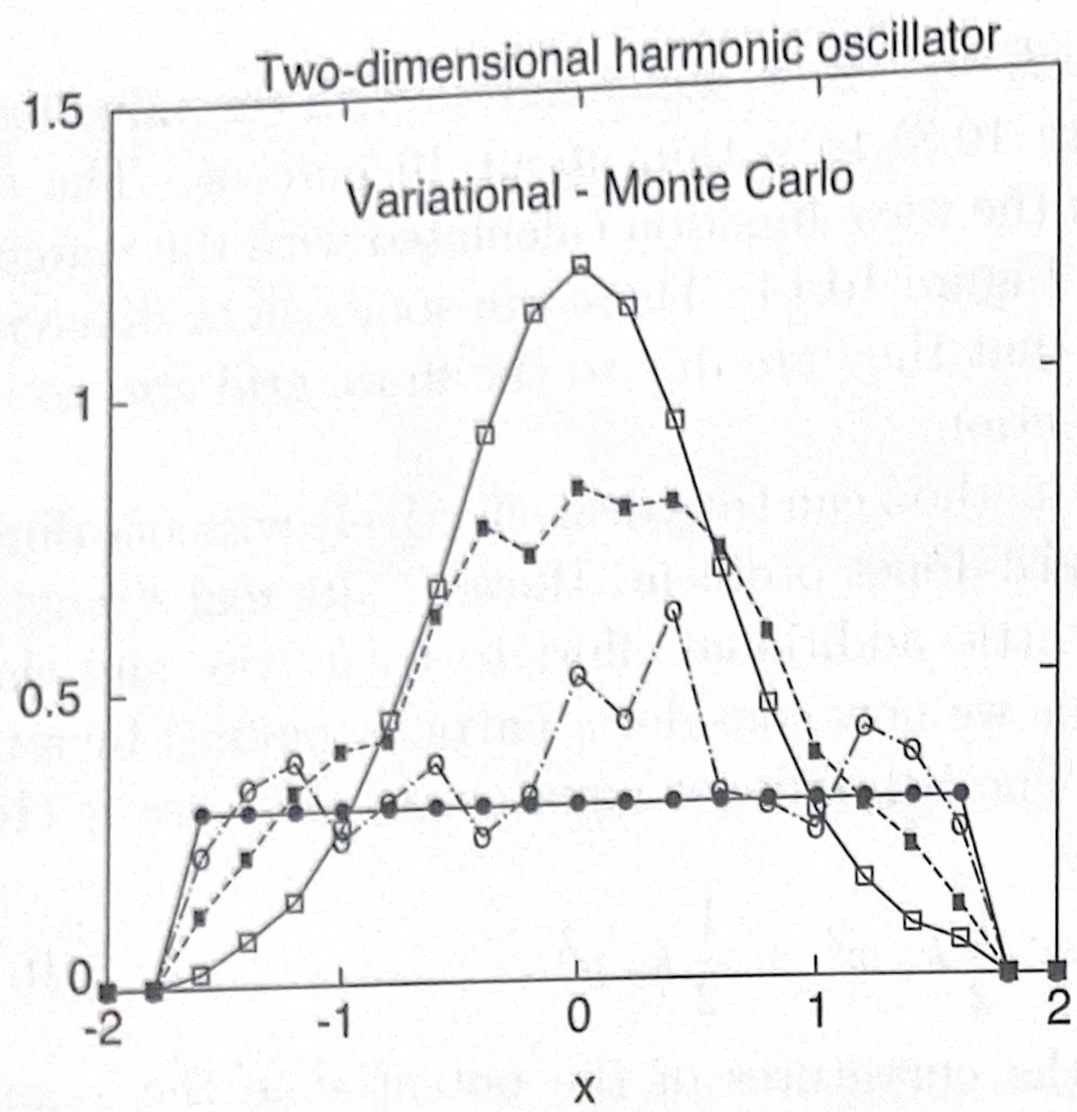

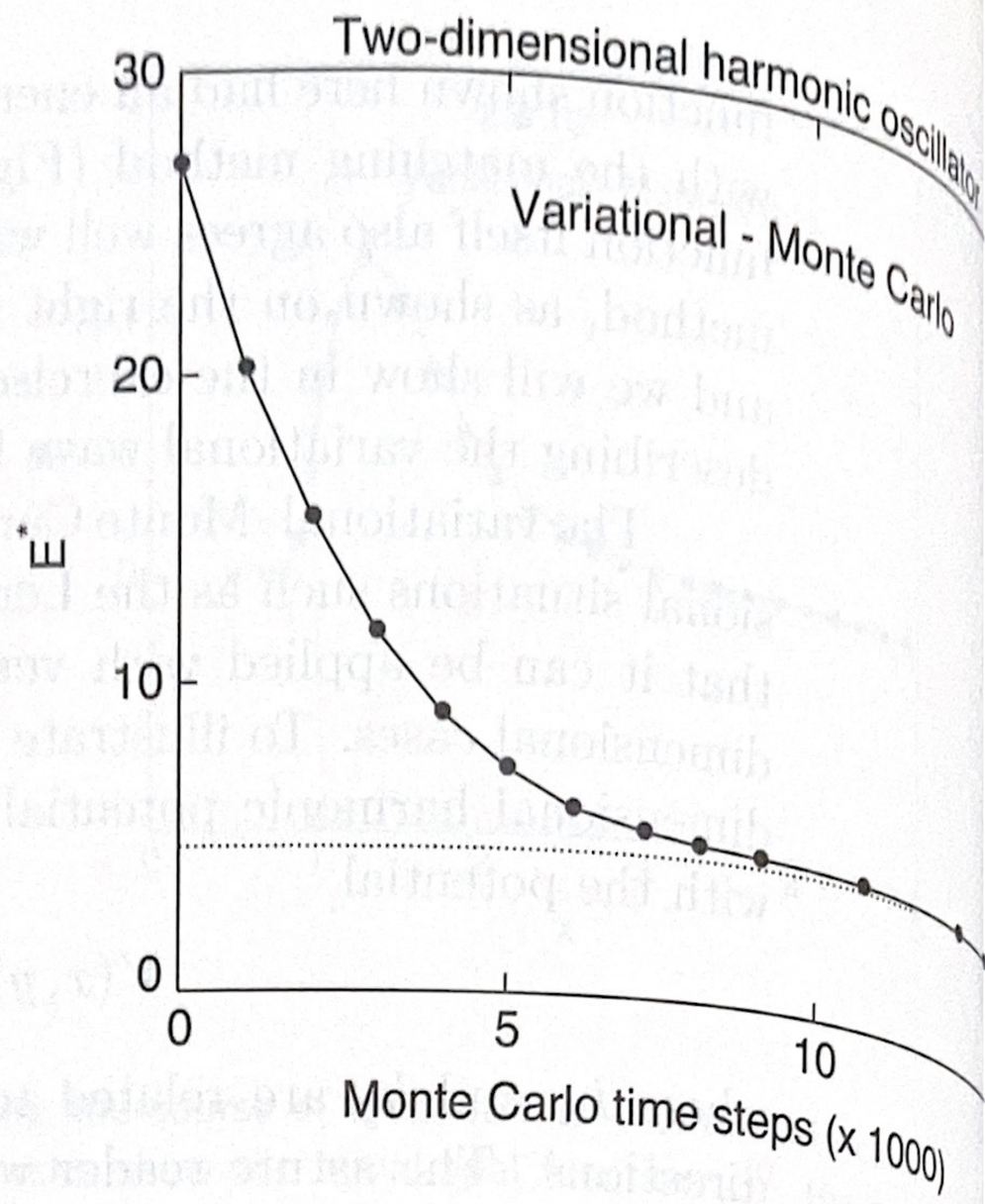

FIGURE 10.15: Left: trial wave functions plotted as $\varphi(x,0)$ as a function of x, at various stages in the variational–Monte Carlo procedure. The filled circles show the initial trial function, and the open circles, filled squares, and open squares show φ after 2000, 5000, and 15,000 Monte Carlo time steps. Right: variation of E^* as the calculation proceeds. The potential energy was (10.29) with $k_x = 10$ and $k_y = 40$, the maximum values of $|x|$ and $|y|$ were 2.0 (so that $\varphi = 0$ outside this region), and the grid size was $\Delta x = \Delta y = 0.2$.

is ~ 4.79, which differs from the exact value $4.743\ldots$ by about 1 percent. We will see in the exercises that this small difference is due to the finite grid size.

While the specific variational–Monte Carlo approach we have described here is fairly well suited for dealing with two- and three-dimensional problems, it is worth considering how the method can be improved. One difficulty is connected with the number of elements of the trial wave function $\varphi_{m,n}$. For the two-dimensional harmonic oscillator example considered above there were ~ 400 grid elements. In order for the Monte Carlo strategy to be successful, it is necessary for each of these $\varphi(m,n)$ to be adjusted many times, and if the number of grid elements is large this can require a long computation. This difficulty can be dealt with in several ways.

First, it pays to make a good choice of the initial trial function, as then an accurate estimate for the true wave function can be reached with fewer Monte Carlo iterations. Here "good" means that φ^0 should have a form close to the true ground-state wave function. We didn't attempt to do this in our calculations here, but it is usually possible to make an informed choice for φ^0. In the exercises we will explore how this can speed up convergence.

Second, in our oscillator example we chose the ranges of x and y to be large enough that the boundaries were far from the region where the wave function was nonzero. This was by design, since ideally the boundary condition $\varphi = 0$ should be applied at $x, y = \pm\infty$. However, this means that there will be many grid elements where φ is extremely small and it would be nice to arrange for the Monte Carlo algorithm to spend less time updating $\varphi(m,n)$ in these regions, since they

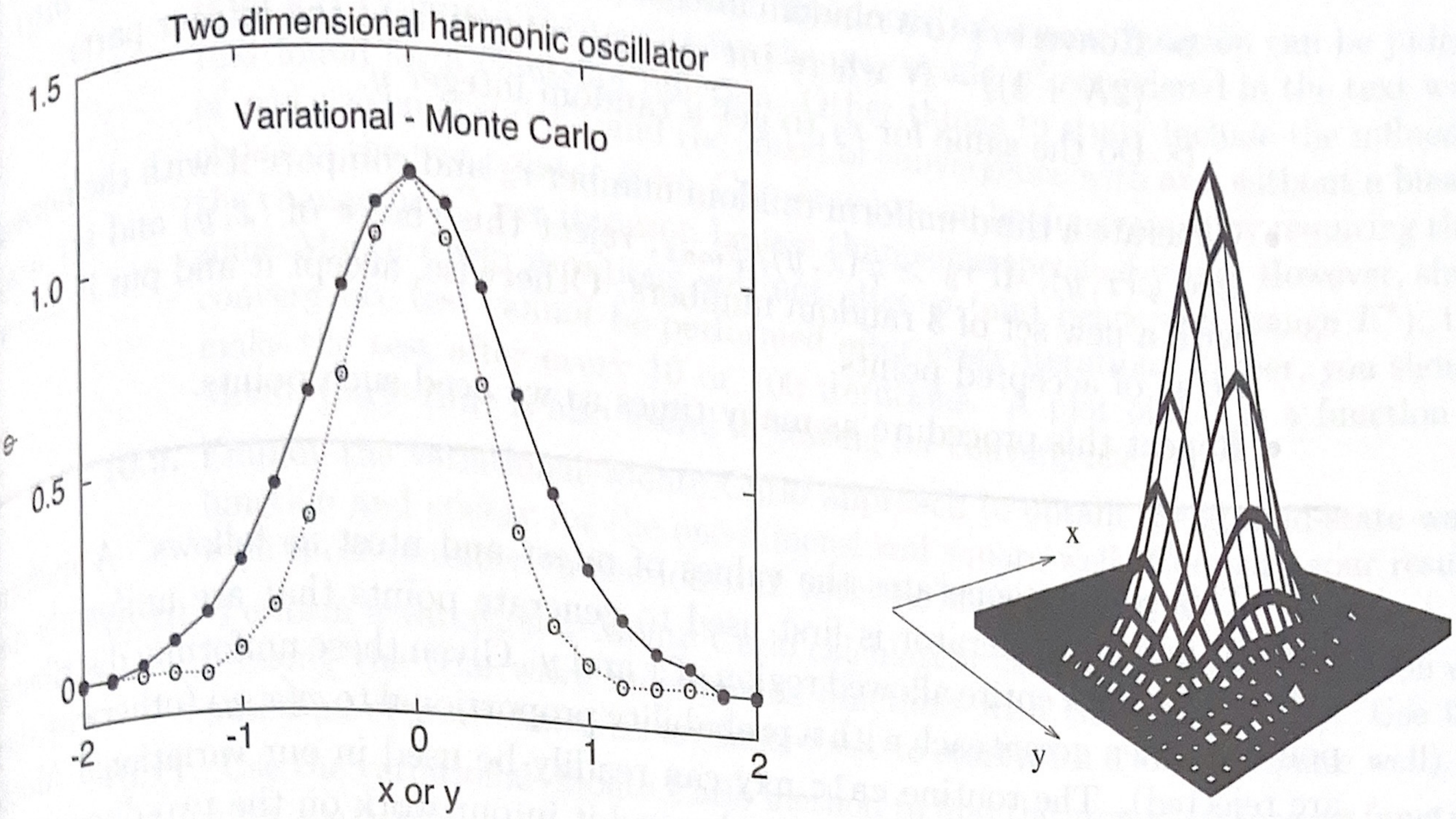

FIGURE 10.16: Left: plot of $\varphi(x,0)$ as a function of x (filled circles) and $\varphi(0,y)$ as a function of y (open circles) for the final trial wave function from Figure 10.15. Right: three-dimensional plot of the wave function.

are not as important as the regions where the wave function is large. This can be accomplished by modifying the way the test locations for the Monte Carlo changes are chosen. In our discussion above we chose the grid element to be considered in the variational procedure, mtest and ntest, at random from the *entire* allowed range of m and n. It would be better to choose the test point with a probability proportional to the value of φ at that point, since then the points where φ is largest would get the most attention from the algorithm. To do this requires that we be able to generate random numbers with a specified distribution. This is a problem that is discussed in Appendix F, where we consider two ways to generate random numbers with a nonuniform distribution. In the problem we are now considering the rejection method is most useful since we do not have an analytic expression for the desired probability function. The method is described in Appendix F, so we will not go into much detail here. A routine that generates mtest and ntest with a probability proportional to $\varphi(m,n)$ is sketched below.

EXAMPLE 10.2 Routine `calc_nxy` to generate random integers according to a specified weighting function

- Assume $\varphi_{max} \equiv \varphi(0,0)$ is the largest value of the trial function. This value is used to normalize $\varphi(x,y)$.
- Generate a point (x,y) randomly.
  - ▷ Generate two uniform random numbers r_1 and r_2 between 0 and 1.

- ▷ Convert r_1 to a random integer x in the range $(-N, N)$ (use $x = int(r_1 \times (2N+1)) - N$ where *int* means truncation to the integer part).
- ▷ Do the same for r_2 to get a random integer y.

- Generate a third uniform random number r_3 and compare it with the normalized $\varphi(x, y)$. If $r_3 > \varphi(x, y)/\varphi_{max}$, reject this choice of (x, y) and try again with a new set of 3 random numbers. Otherwise, accept it and put it into an array of accepted points.
- Repeat this procedure as many times as we need such points.

This routine generates the values of mtest and ntest as follows. A uniform random number generator is first used to generate points that are uniformly distributed over the entire allowed region of x and y. Given these uniformly distributed points we then *accept* each with a probability proportional to $\varphi(x, y)$ (otherwise they are rejected). The routine `calc_nxy` can readily be used in our variational–Monte Carlo calculations. In fact, we already used it in our work on the two-dimensional harmonic oscillator! In the exercises we will consider how much it speeds up the calculation as compared with simply choosing mtest and ntest uniformly.[27]

A third useful modification of the variational–Monte Carlo method involves the manner in which we represent the trial functions. So far we have taken a direct, but in some ways crude approach by simply storing the value of φ at each grid site separately. A different strategy, which is in the spirit of a Fourier decomposition, would be to write the trial function as a sum of *basis* functions.[28] For example, with the harmonic oscillator we might choose the basis set to be Gaussian-like functions with different widths. The important point is that these functions be orthogonal so that an arbitrary trial function can be written uniquely in a form such as

$$\varphi(x, y) = \sum_k a_k \, b_k(x, y) \ , \tag{10.30}$$

where $b_k(x, y)$ are the basis functions and the coefficients a_k specify the overlap between the trial wave function φ and the different basis functions. The variational procedure then involves adjusting the values of these coefficients so as to minimize the effective energy E^*. This can again be accomplished using a Monte Carlo approach.

EXERCISES

10.8. Write a program to implement the variational–Monte Carlo approach and apply it to the two-dimensional harmonic oscillator. Study how the choice of initial trial wave function affects the number of Monte Carlo steps required to obtain

---

[27] In most cases it is advisable to initially choose mtest and ntest from a uniform distribution. This prevents errors (i.e., zeros) in the initial trial wave function from unduly restricting the form of later trial functions. After the trial function begins to resemble the true wave function, you can then switch to choosing from a biased distribution and thereby speed up the final convergence of the Monte Carlo algorithm.

[28] We will encounter such basis functions in detail later in this chapter.

a "good" wave function. Here the "goodness" of a wave function can be judged from E^*. Compare the results for the very crude φ^0 considered in the text with that found for a Gaussian function. Other things to study include the influence of grid size on φ and E^* and the speed of convergence with and without a biased choice of the test points. *Hint:* Convergence can be determined by requiring that the change in E^* per iteration be less than some specified value. However, since some Monte Carlo iterations will not alter φ (and hence not change E^*), the convergence test cannot be performed after every iteration. Rather, you should make the test after every 10 or 100 iterations. A plot of E^* as a function of Monte Carlo time is also useful in testing for convergence.

10.9. Employ the variational–Monte Carlo approach to obtain the ground-state wave function and energy for the one-dimensional square well. Compare your results with those obtained in Section 10.2 with the shooting method.

***10.10.** Perform a variational–Monte Carlo calculation using an approach based on expressing the trial wave functions as functions with the form (10.30). Use the potential of your choice (it might be best to start with a simple square well).

10.11. Use the variational–Monte Carlo method to find the ground-state wave function for a particle in a box in three dimensions. Compare the results for boxes with different wall potentials.

10.12. Employ the variational–Monte Carlo method to calculate the ground-state energy and wave function of the anharmonic oscillator whose potential is given by $V(x) = x^4$.

***10.13.** The variational theorem as stated at the beginning of this section concerns the ground-state energy and wave function. That is why all of the problems in this section have (so far) been concerned with the ground state. However, the method can also be used to deal with the excited states in the following way. The wave functions of the ground and excited states form a complete orthogonal set of basis functions. If the variational function φ is orthogonal to the ground-state wave function, then the final result of a variation calculation will be the wave function of the first excited state and E^* will be the energy of this state. While this may sound simple in principle, a difficulty in practice is that even though φ^0 may be constructed so as to be orthogonal to the ground state, the Monte Carlo changes may spoil this orthogonality.

Investigate this problem by using the variational–Monte Carlo method to estimate the first excited state of a particle in a square well. The challenging part of the problem is to ensure in some manner that after each Monte Carlo modification of φ, this function is still orthogonal to the ground-state wave function.

10.5 TIME-DEPENDENT SCHRÖDINGER EQUATION: DIRECT SOLUTIONS

In the past few sections we have explored several approaches for solving the *time-independent* Schrödinger equation. We have seen how to calculate the wave functions of the ground and excited states for different potentials in one, two, and three dimensions. However, to appreciate some of the most interesting aspects of quantum mechanics it is necessary to consider the time dependence of the wave function. This will be our aim in the remainder of this chapter. Our first goal is to treat problems such as wave-packet propagation in free space, reflection from a potential step, and tunneling through a barrier.

The time-dependent Schrödinger equation has the form

$$-\frac{\hbar^2}{2m}\nabla^2\psi + V(\vec{r})\,\psi = \imath\hbar\frac{\partial\psi}{\partial t}\,, \tag{10.31}$$

where t is the time and again $\imath \equiv \sqrt{-1}$. Dealing with this problem in three dimensions is a formidable computational problem, so we consider the (numerically) simpler case of one dimension. We then have

$$-\frac{\hbar^2}{2m}\frac{\partial^2\psi}{\partial x^2} + V(x)\,\psi = \imath\hbar\frac{\partial\psi}{\partial t}\,, \tag{10.32}$$

where now ψ is a function of x and t. We will explore a number of ways of dealing with this problem. One is a spectral method, much like the one we employed in connection with waves on a string in Chapter 6; we will describe that approach in Section 10.7. Here and in the next section (10.6) we consider somewhat more direct attacks.

The first and main approach we consider is a rather straightforward extension of the centered difference method used in Chapter 6. It is instructive to rewrite (10.32) in the form

$$\imath\hbar\frac{\partial\psi}{\partial t} = \mathcal{H}\,\psi\,, \tag{10.33}$$

where the Hamiltonian operator is defined by

$$\mathcal{H} \equiv -\frac{\hbar^2}{2m}\frac{\partial^2}{\partial x^2} + V(x)\,. \tag{10.34}$$

Constructing finite difference equations from these relations requires that we deal with complex quantities.[29] Thus, let us denote the real part of ψ by R and the imaginary part by I,

$$\psi(x,t) = R(x,t) + \imath\,I(x,t)\,. \tag{10.35}$$

Equation (10.33) then breaks into

$$\frac{\partial R}{\partial t} = \left(-\frac{1}{2}\frac{\partial^2}{\partial x^2} + V(x)\right) I \tag{10.36}$$

$$\frac{\partial I}{\partial t} = \left(\frac{1}{2}\frac{\partial^2}{\partial x^2} - V(x)\right) R\,, \tag{10.37}$$

where the factors involving $\hbar$ and m have (according to common convention for such problems) both been set equal to unity.[30] We then approximate both the spatial and the time derivatives as centered differences. For example,

$$\frac{\partial^2 R(x,t)}{\partial x^2} \approx \frac{R(x+\Delta x,t) - 2R(x,t) + R(x-\Delta x,t)}{(\Delta x)^2}\,, \tag{10.38}$$

[29] Unlike the time-independent problems considered in the previous sections, for most time-dependent problems we can not avoid a complex wave function.

[30] This is a slightly different convention than what we used in discussing the time-independent Schrödinger equation in earlier sections.

and
$$\frac{\partial I(x,t)}{\partial t} \approx \frac{I(x,t+\Delta t/2) - I(x,t-\Delta t/2)}{\Delta t} . \tag{10.39}$$

Inserting these into (10.37) yields an expression for $I(x,t+\Delta t/2)$ in terms of $I(x,t-\Delta t/2)$, $R(x \pm \Delta x, t)$, and $R(x,t)$. After a little rearranging we get

$$\begin{aligned} I(x,t+\Delta t/2) \approx\ & I(x,t-\Delta t/2) \\ & + \frac{\Delta t}{2(\Delta x)^2}\,[R(x+\Delta x,t) - 2R(x,t) + R(x-\Delta x,t)] \\ & - (\Delta t)V(x)R(x,t) . \end{aligned} \tag{10.40}$$

If we now discretize space by taking $x_m = m\Delta x$, and use the values of R and I at x_m, it is evidently most convenient, according to (10.40), to evaluate $R(x,t)$ at $x = x_m$ and $t = n\Delta t$ while $I(x,t)$ is evaluated at $x = x_m$ and at the *shifted* times $t = (n \pm \frac{1}{2})\Delta t$. The corresponding expression for the real part of the wave function R using the shifted discrete times for R and I is

$$\begin{aligned} R(x,t+\Delta t) \approx\ & R(x,t) - \frac{\Delta t}{2(\Delta x)^2}\,[I(x+\Delta x,t+\Delta t/2) - 2I(x,t+\Delta t/2) \\ & + I(x-\Delta x,t+\Delta t/2)] - (\Delta t)V(x)I(x,t+\Delta t/2) . \end{aligned} \tag{10.41}$$

We are thus evaluating the real and imaginary parts of $\psi(x,t)$ in a *leapfrog* fashion at "staggered" times. However, this presents no practical difficulty, and in fact one can show that the numerical errors made in this method are locally of order $(\Delta t)^3$, the same order as with the second-order Runge-Kutta methods. This leapfrog approach also has the very important property of conserving the normalization of the wave function; that is, the integral of $\psi^*\psi$ over all space is conserved.

While the leapfrog method just described is suitable for carrying out the calculations to obtain all of the results that we show later in this section, we will now describe a second direct approach which is related to the general matrix formulation that we discussed earlier in this chapter. This second method provides an important lesson in dealing with linear equations containing Hermitian operators such as $\mathcal{H}$. Although (10.33) has the appearance of a simple first-order differential equation involving the time dependence of ψ, things are complicated by the fact that $\mathcal{H}$ is an operator rather than a number. Ignoring that fact for a moment, (10.33) has the formal solution

$$\psi(x,t) = \exp(-\imath\, t\, \mathcal{H}/\hbar)\, \psi(x,0) , \tag{10.42}$$

where $\psi(x,0)$ is the wave function at $t = 0$. Thus, if we know $\psi(x,0)$, we can *formally* calculate the behavior at all future times using (10.42). However, this formal solution is not as useful as we might hope because of the operator $\mathcal{H}$ in the exponent. To be clear on what it means mathematically to have an operator expression of this kind, it is useful to rewrite (10.42) using the Taylor expansion of the exponential factor

$$\exp(-\imath\, t\, \mathcal{H}/\hbar)\, \psi = \left(1 - \frac{\imath\, t}{\hbar}\mathcal{H} - \frac{t^2}{2\,\hbar^2}\mathcal{H}^2 \ldots\right) \psi , \tag{10.43}$$

where $\mathcal{H}^n$ means that the operator $\mathcal{H}$ is applied n times in succession. The problem comes when we have to evaluate terms such as $\mathcal{H}^2\psi$. Recalling the definition of $\mathcal{H}$, we see that such a term expands to give

$$\mathcal{H}^2\,\psi \;=\; \mathcal{H}\,\mathcal{H}\,\psi \;=\; \left[-\frac{\hbar^2}{2m}\frac{\partial^2}{\partial x^2} + V(x)\right]\left[-\frac{\hbar^2}{2m}\frac{\partial^2}{\partial x^2} + V(x)\right]\psi\,. \tag{10.44}$$

Difficulties now arise from the fact that the two terms that make up $\mathcal{H}$ do not commute; that is, the order of operation is important. We cannot simply switch the order with which we apply the derivative term in $\mathcal{H}$ (the kinetic energy piece) and the potential energy part (which, in general, depends on position). This makes dealing with the time-dependent Schrödinger equation more complicated than dealing with a simple first-order differential equation such as those discussed in Chapter 1.

While (10.42) is a perfectly fine formal solution, it is not of much practical use since the expansion (10.43) involves a very large (infinite) number of terms. However, this formal solution does suggest a way to proceed numerically. Let us consider applying the formal solution over a very small time interval. Indeed, let us discretize time in steps Δt; using (10.42) we obtain

$$\psi(x, t+\Delta t) \;=\; \exp(-\imath\,\Delta t\,\mathcal{H}/\hbar)\,\psi(x,t)\,. \tag{10.45}$$

But, you might ask, how can this be a useful approach in view of the difficulties with the expansion (10.43)? The reason we could have some optimism with regard to (10.45) is that a small value of Δt will make the higher-order terms in the expansion (10.43) small. Let us assume for now that these terms can be made small enough that we can stop at the term linear in $\mathcal{H}$, which yields[31]

$$\psi(x, t+\Delta t) \;\approx\; (1 - \imath\,\Delta t\,\mathcal{H}/\hbar)\,\psi(x,t) \;=\; \left[1 + \frac{\imath\Delta t}{2}\frac{\partial^2}{\partial x^2} - \imath\,\Delta t\,V(x)\right]\psi(x,t)\,, \tag{10.46}$$

where in the last step we have again assumed $\hbar = 1$ and $m = 1$. Given (10.46), a natural way to proceed is to discretize space into units of size Δx and write the wave function as $\psi(m,n) \equiv \psi(m\Delta x, n\Delta t)$. Expressing the second partial derivative in the usual finite-difference form, (10.46) becomes

$$\psi(m, n+1) \;\approx\; \psi(m,n) + \frac{\imath\,\Delta t}{2}\left[\frac{\psi(m+1,n) + \psi(m-1,n) - 2\,\psi(m,n)}{(\Delta x)^2}\right] - \imath\,\Delta t\,V(m)\,\psi(m,n)\,. \tag{10.47}$$

Hence, given $\psi(m,n)$ it appears that we can readily calculate $\psi(m,n+1)$, the wave function at the next time step. However, this approach contains two flaws.

The first flaw is this procedure is numerically unstable! The effects of small round-off and other types of errors (due, for example to the higher-order terms we have neglected) grow rapidly with time, essentially because of the exponential factor in (10.45) from which this finite-difference equation was derived. Amazingly,

[31] This could also be obtained by expressing (10.33) in finite-difference form, but we will have further use for (10.45) moment.

this instability can be cured by rewriting (10.45) so as to, in a sense, propagate *backward* in time,

$$\psi(x,t) = \exp(+\imath\,\Delta t\,\mathcal{H}/\hbar)\,\psi(x,t+\Delta t) \approx (1 + \imath\,\Delta t\,\mathcal{H}/\hbar)\,\psi(x,t+\Delta t)\,. \quad (10.48)$$

We will not go into the details of precisely why the scheme (10.48) leads to numerical stability, but leave that for interested readers to explore using the references. However, this stability does come at a price; when (10.48) is converted into finite difference form one is led to the following set of the finite-difference equations

$$\begin{aligned}\psi(m,n) &\approx \psi(m,n+1) \\ &- \frac{\imath\,\Delta t}{2}\left[\frac{\psi(m+1,n+1)+\psi(m-1,n+1)-2\,\psi(m,n+1)}{(\Delta x)^2}\right] \\ &+ \imath\,\Delta t\,V(m)\,\psi(m,n+1)\,.\end{aligned} \quad (10.49)$$

Comparing this with (10.47) we find that it is an *implicit* relation for $\psi(m,n+1)$. That is, we cannot use (10.49) to express $\psi(m,n+1)$ solely in terms of the wave function at time step $n+1$, but we are stuck with terms of the form $\psi(m',n+1)$ with $m' \neq m$ in the expression for $\psi(m,n+1)$. Hence, we cannot just step through the values of m and use (10.49) to calculate the wave function at the next time step. We must instead solve a system of algebraic equations, and this amounts to a matrix formulation as described earlier in this chapter.

However, even this price is not all that we must pay. Equations (10.47) and (10.49) both violate a fundamental property of quantum mechanics called *unitarity*. The Schrödinger equation preserves the proper normalization of a wave function, that is, the total probability for finding a particle somewhere in space must always be unity.[32] It turns out that $(1 - \imath\,\Delta t\,\mathcal{H}/\hbar)$, the time evolution operator in (10.46), is *not* unitary, and the same is true of (10.48). We must therefore devise a different strategy.

A numerically stable approach that does satisfy unitarity involves writing the exponential factor in (10.45) in what is known as the Cayley form

$$\exp(-\imath\,\Delta t\,\mathcal{H}/\hbar) \approx \frac{1 - \imath\,\Delta t\,\mathcal{H}/2\hbar}{1 + \imath\,\Delta t\,\mathcal{H}/2\hbar}\,. \quad (10.50)$$

We will leave it to the reader to show that to lowest order in $\mathcal{H}$ (in a Taylor expansion), this is equal to both $1 - \imath\,\Delta t\,\mathcal{H}$ and $(1 + \imath\,\Delta t\,\mathcal{H})^{-1}$, which are the key factors in (10.46) and (10.48). However, these three ways of approximating the exponential factor $\exp(-\imath\,\Delta t\,\mathcal{H})$ are *not* equivalent with regard to maintaining unitarity, as can be seen in the following way. Using (10.50) to propagate our wave function forward in time we have

$$\psi(x,t+\Delta t) \approx \frac{1 - \imath\,\Delta t\,\mathcal{H}/2\hbar}{1 + \imath\,\Delta t\,\mathcal{H}/2\hbar}\,\psi(x,t)\,. \quad (10.51)$$

[32] The conservation of probability is ensured by the *unitarity* of the operator $\exp(-\imath t\mathcal{H}/\hbar)$ in (10.42), which is the direct result of the fact that $\mathcal{H}$ is Hermitian.

From (10.51) we first obtain

$$\left[1 + \frac{\imath\,\Delta t\,\mathcal{H}}{2\hbar}\right]\psi(x, t+\Delta t) = \left[1 - \frac{\imath\,\Delta t\,\mathcal{H}}{2\hbar}\right]\psi(x,t)\,. \tag{10.52}$$

We now replace $\mathcal{H}$ by (10.34), convert everything to finite-difference form, and discretize space and time so that $\psi(m,n) \equiv \psi(m\Delta x, n\Delta t)$. After rearranging a few terms we get

$$\begin{aligned}\psi(m+1,n+1) &+ [2\imath\lambda - 2(\Delta x)^2 V(m) - 2]\,\psi(m,n+1) + \psi(m-1,n+1) \\ &= -\psi(m+1,n) + [2\imath\lambda + 2(\Delta x)^2 V(m) + 2]\,\psi(m,n) - \psi(m-1,n)\,,\end{aligned} \tag{10.53}$$

where for notational convenience we define $\lambda \equiv 2(\Delta x)^2/\Delta t$. The system of equations (10.53) has a form that is different from anything we have encountered in previous chapters. Most importantly, they cannot be rewritten so as to express $\psi(m,n+1)$ solely in terms of $\psi(m,n)$. Hence, we cannot simply loop through the values of m and compute each $\psi(m,n+1)$ in a straightforward manner. Instead, we have an *implicit* numerical problem, which means that the value of $\psi(m,n+1)$ for a particular value of m depends on $\psi(m',n+1)$, where $m' \neq m$. That is, we have a set of algebraic equations (which can again be cast as a matrix problem) that must be solved to obtain the wave function at the next time step.

As noted earlier in this chapter, many eigenvalue problems can be expressed in matrix form, with the solution then requiring that a matrix be diagonalized or inverted. In the present case we must invert the matrix whose coefficients can be read from (10.53). The bad news is that this will be a *large* matrix. In the particular problems we will consider below, the number of grid elements along x is typically 1000, so the associated matrix is 1000×1000 in size. This is a formidable computational problem, especially when we realize that such a matrix must be inverted for *each* time step! Fortunately, there is some good news: most of the elements of this matrix are zero. If we examine (10.53) we see that the equation for $\psi(m,n+1)$ involves just $\psi(m \pm 1, n+1)$, and no other values of ψ [except for itself, $\psi(m,n+1)$]. Thus, each row of our matrix has only three nonzero elements. Since one of these is on the diagonal and the other two are just one space away, this matrix is *tridiagonal*. Such matrices arise often in numerical work, since as in the present case the effectively "local" nature of the underlying differential equation gives rise naturally to this matrix structure. As you might expect, the large number of the zeros in the matrix can be used to our advantage. There are several algorithms which take advantage of the special form and give good results. A popular approach is the *Crank-Nicholson* method, which is described in detail in the paper by Goldberg, Schey, and Schwartz in the references (this method was also discussed in detail in the first edition of this book). The Crank-Nicholson approach and the leapfrog method described earlier in this section can both be used for the calculations we describe in the remainder of this section.

We now consider a few examples of the time-dependent behavior of ψ as calculated using one of the algorithms described above. The primary initial condition

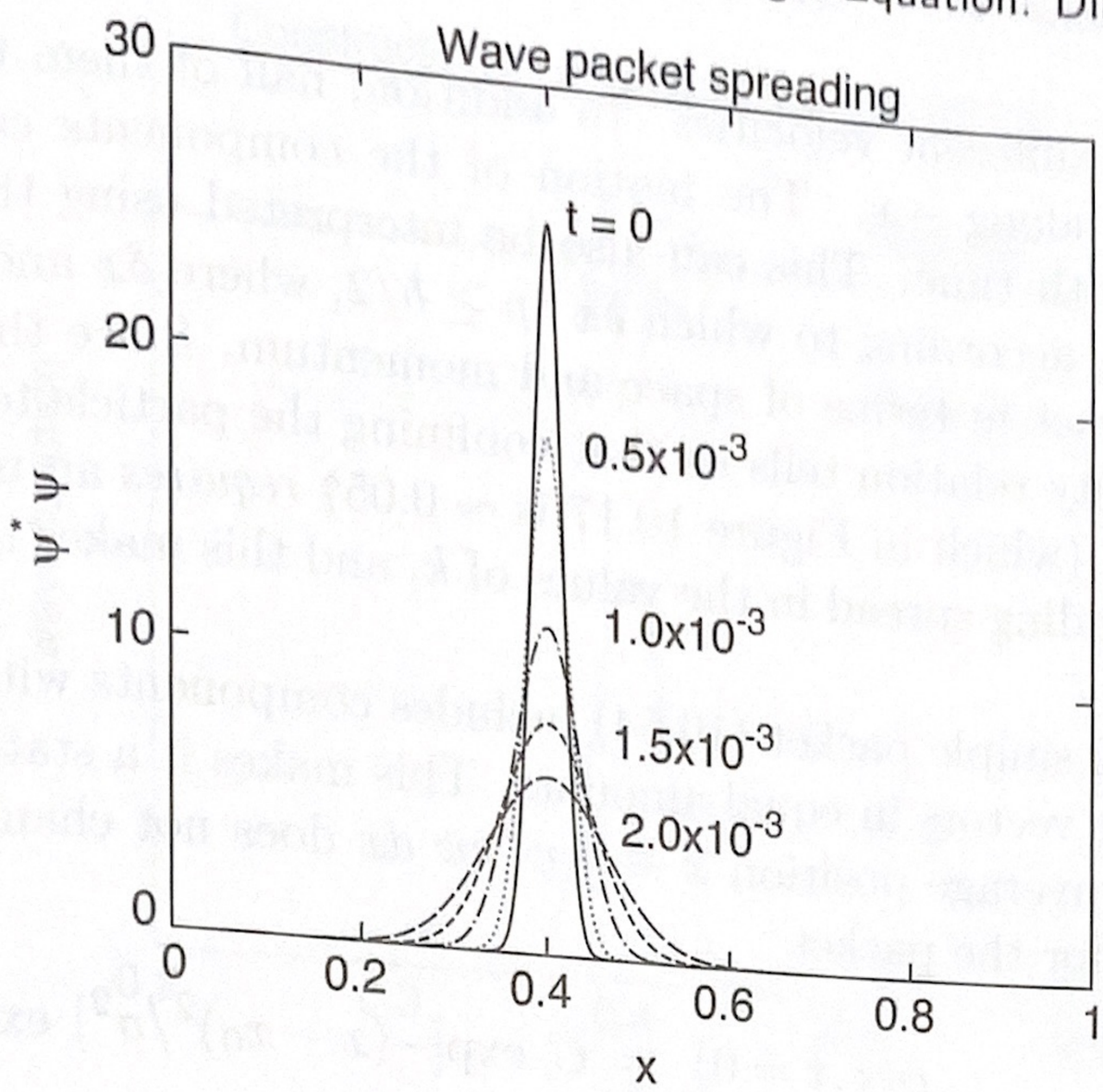

FIGURE 10.17: Time-dependent behavior of a Gaussian wave packet. The initial wave packet ($t = 0$) is given by (10.54) with $x_0 = 0.4$ and $\sigma^2 = 1 \times 10^{-3}$. The wave function at later times (the time values are given in the figure) is seen to spread out in space. For this calculation we used $\Delta x = 0.0005$ with the boundary condition $\psi = 0$ applied at $x = 0$ and $x = 1$. We also took $\Delta t = 5 \times 10^{-7}$ so that $\lambda = 2(\Delta x)^2/\Delta t = 1$.

in these calculations is the initial wave function. In all of the examples considered below we assume a Gaussian form for ψ at $t = 0$, so that our initial wave function is given by

$$\psi(x, t = 0) \;=\; C \exp[-(x - x_0)^2/\sigma^2] \,, \tag{10.54}$$

where the center of the packet is at x_0, its width is σ, and the factor C is chosen to satisfy the normalization condition on ψ. A plot of such a wave packet is shown by the solid curve in Figure 10.17. This wave function is not stable with time; we see from Figure 10.17 that it broadens as t increases. Since our algorithm maintains unitarity[33] a broader wave function must have a lower value at the peak, as also seen in Figure 10.17.

The physics responsible for this wave-packet spreading can be understood by recalling that we are dealing with an equation much like the wave equation considered in Chapter 6. The Gaussian wave packet (10.54) can be decomposed into (i.e., written as) a sum of plane waves of the form e^{ikx}. These plane waves are essentially just Fourier components[34] whose amplitudes are chosen so that they add up to give the Gaussian packet (10.54) at $t = 0$. However, each component is a wave that travels along the system. These waves have different wave vectors, k,

[33] It is a good idea to periodically check that $\int \psi^* \psi \, dx = 1$, as this provides a strong test that your program does not contain any subtle bugs. The wave functions shown in Figure 10.17 and in later figures all satisfy this test. With the leapfrog algorithm, we need to sum the squares of the real and imaginary parts evaluated half a time step apart to obtain ψ^2, but this usually presents no practical problem.

[34] Just as the sines and cosine standing waves are the Fourier components for waves on a string.

and thus different velocities. In addition, half of them travel in the $+x$ direction and half along $-x$. The motion of the components causes the wave packet to spread with time. This can also be interpreted using the Heisenberg uncertainty principle, according to which $\delta x\, \delta p \geq \hbar/2$, where δx and δp are the widths of the wave packet in terms of space and momentum. Since the momentum $p = \hbar k$, the uncertainty relation tells us that confining the particle to an initial wave packet of width δx (which in Figure 10.17 is ~ 0.05) *requires* an uncertainty in k, that is, a corresponding spread in the values of k, and this makes the packet spread out with time.

The simple packet (10.54) includes components with both positive and negative wave vectors in equal amounts. This makes it a stationary packet in the sense that the average position $\overline{x} \equiv \int \psi^* x \psi\, dx$ does not change with time. This is not the case for the packet

$$\psi(x, t = 0) \;=\; C \exp[-(x - x_0)^2/\sigma^2] \exp[\imath\, k_0\, x] \;, \tag{10.55}$$

which is just our original Gaussian function multiplied by a plane wave with wave vector k_0. This wave function, which is complex, can also be written as the sum of components with a range of k values, but with the range now centered around k_0. As a result, this packet travels with an average velocity $v_0 = \hbar k_0/m$. It is interesting to compare it with the stationary wave functions considered above. While we only show $\psi^*\psi$ in Figure 10.17, you can see from (10.54) that at $t = 0$ this is also just the square of the real part of ψ and that the imaginary part is zero. Our propagating packet is a little more complicated, as can be seen from Figure 10.18. While $\psi^*\psi$ has the same simple Gaussian shape, the real and imaginary parts of ψ oscillate rapidly. This oscillation is due to the factor $\exp(\imath k_0 x)$ in (10.55). In fact, for these oscillations to be prominent, we must choose k_0 and σ appropriately; i.e., we need $\sigma \gg 1/k_0$. This choice also makes $\hbar k_0$ a well-defined mean momentum of the packet, as the width of the wave packet in k-space is proportional to $1/\sigma$.

In carrying out the calculations, we should also not forget the stability and accuracy requirements. As in any numerical solution of initial-value problems, the calculated wave function can propagate at a speed that is no faster than $\Delta x/\Delta t$, where Δx and Δt are the discrete steps in space and time, respectively. Since the wave packet moves on average with a speed $v_0 = \hbar k_0/m$, we must have $\Delta x/\Delta t \geq \hbar k_0/m$ for the calculation to keep up with the packet. Also an accurate description of the oscillating real and imaginary parts in the packet requires $\Delta x \ll \lambda_0$ where $\lambda_0 = 2\pi/k_0$ is the average wavelength.

The results of our propagation program when applied to this packet are shown in Figure 10.19. Here the packet in Figure 10.18 was allowed to move in a region with $V = 0$. That is, we had a freely moving particle. We will leave it to the exercises to show that this motion has the expected velocity. You should notice that the height of the propagating packet decreased as it moved. This is due to the wave-packet spreading we noted in connection with the stationary packet in Figure 10.17. The uncertainty relation tells us that *all* such packets will spread with time. If we had chosen a larger value of k_0, the velocity of the packet would be larger, and since the rate of spreading would be the same, the packet would better

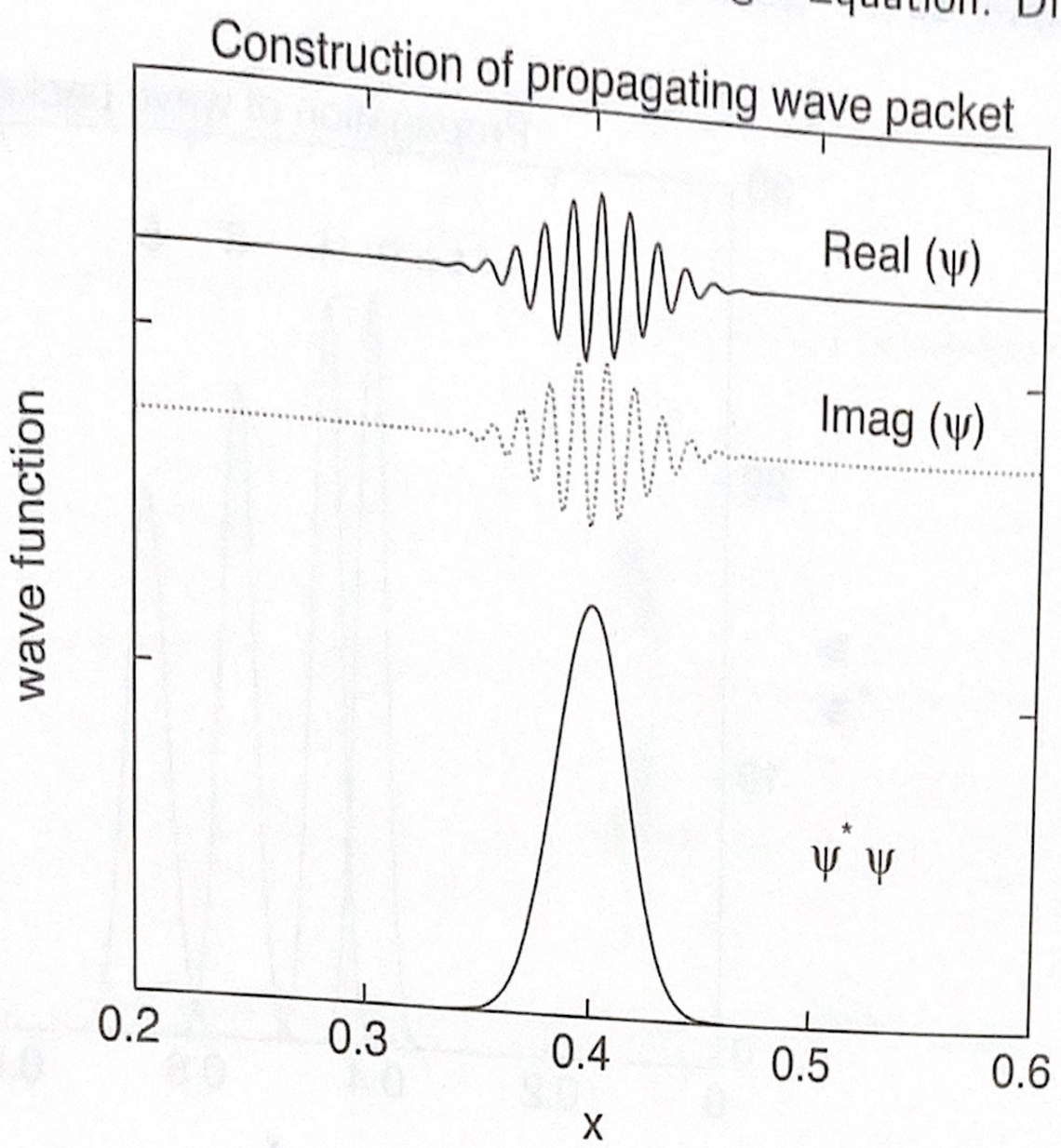

FIGURE 10.18: Composition of a propagating wave packet. For this packet we took $k_0 = 500$, $x_0 = 0.4$, and $\sigma^2 = 0.001$.

maintain its amplitude for a given distance traveled. We will investigate this in the exercises.

We can use this propagating wave packet to study a wide variety of problems involving reflection, transmission, and tunneling. The programming is essentially identical to that required to treat motion in a flat ($V = 0$) potential region. The only difference is that we must employ the appropriate potential function $V(x)$ in the calculation. We first consider an encounter with a potential wall; that is, we let our wave packet begin in a region with $V = 0$ and propagate toward a region where V is very large. Figure 10.20 shows the behavior with a wall located at $x = 0.6$. The potential for $x \geq 0.6$ was 1×10^6. This was much greater than the average energy of the wave packet, $E_{\text{packet}} = \hbar^2 k_0^2/2m$, which in this case was 1.25×10^5. Hence, the particle did not have enough energy to classically propagate into the region $x \geq 0.6$ and was instead completely reflected.

In some respects the reflection process resembles the behavior of a wave pulse on a string when it encounters the end of the string. However, the details in the quantum case are somewhat different as can be seen from the detailed plots on the right in Figure 10.20. The rapid oscillations of $\psi^*\psi$ are especially striking and are often not appreciated from the usual analytic treatments of the reflection process.

Another interesting case is a potential cliff. We again consider a wave packet that, as in Figure 10.20, was incident from a region in which $V = 0$. Now, however, the potential *dropped* to $V = -10^6$ when $x \geq 0.6$. From Figure 10.21 we see that while some of the packet was transmitted, a comparable amount was also reflected. That is, there was a nonzero probability for the particle to be reflected from the cliff! This is a nice illustration of the wave nature of quantum mechanics, since such behavior would never be found in classical mechanics. In a sense we could

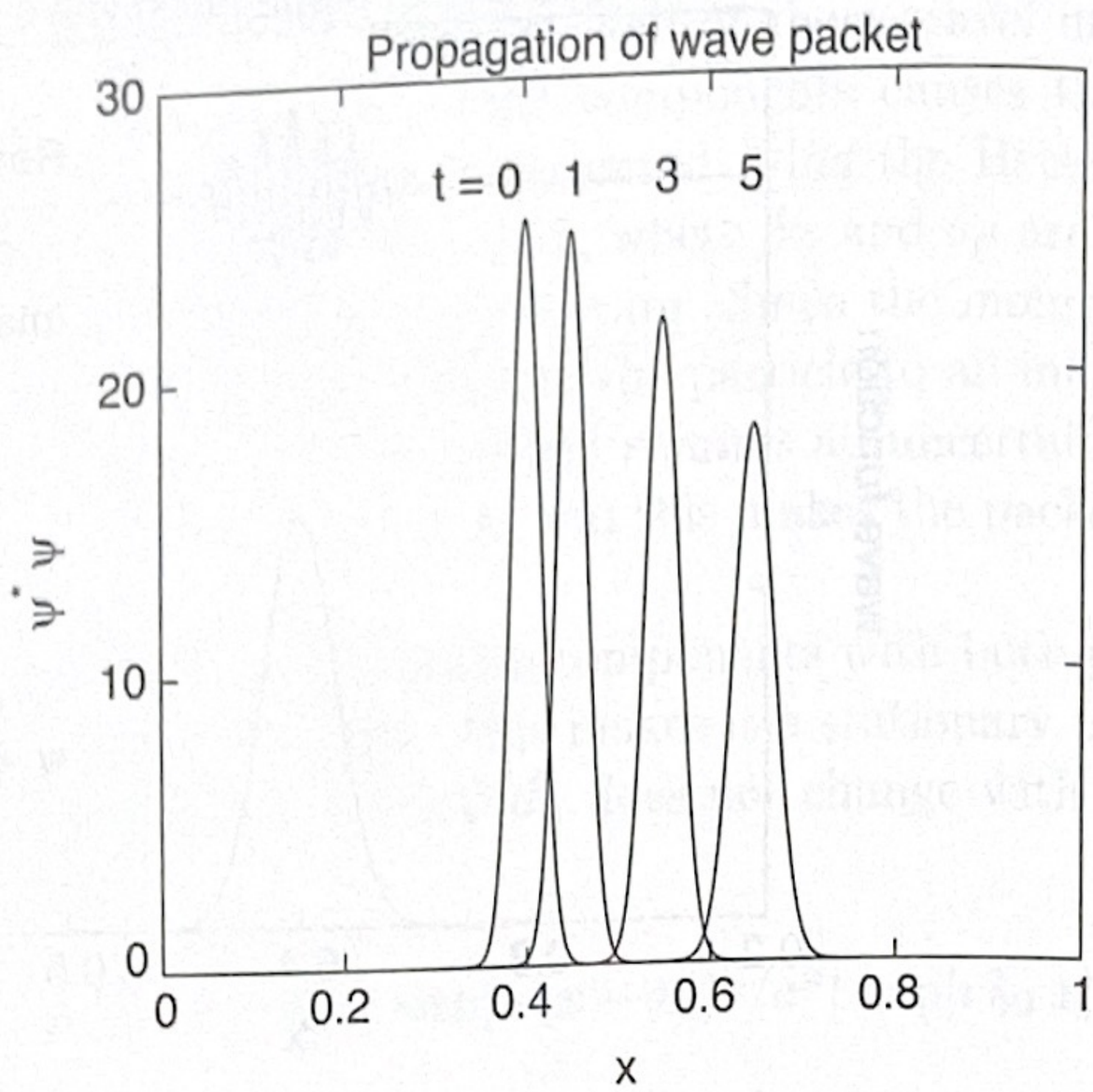

FIGURE 10.19: Wave packet (10.55) from Figure 10.18 propagating in a region with $V = 0$. The time values given in the figure are to be multiplied by $\times 10^{-4}$. We used $\Delta x = 0.0005$ and $\Delta t = 5 \times 10^{-7}$ in the calculation.

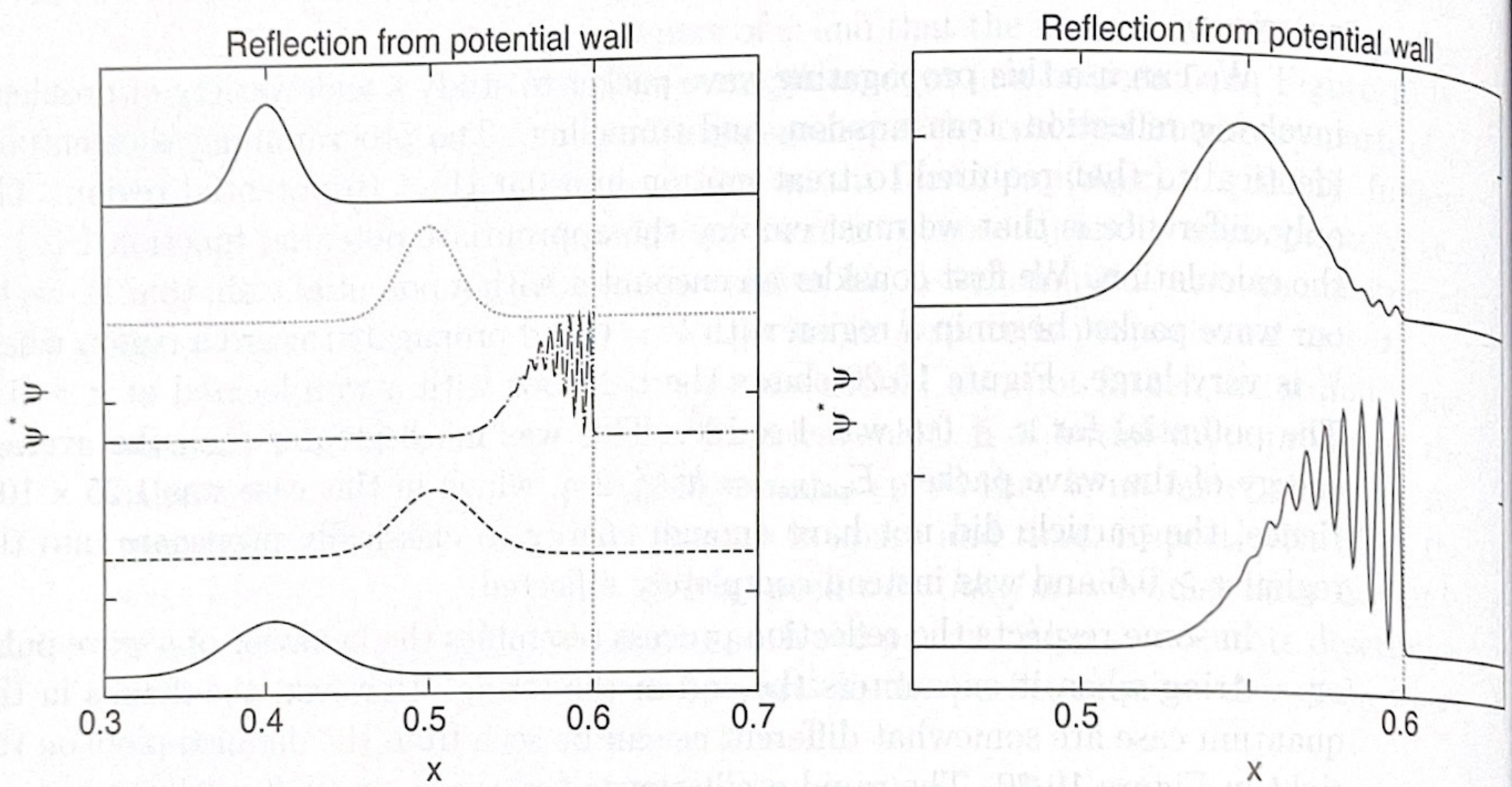

FIGURE 10.20: Wave packet reflecting from a wall, which is indicated by the vertical dotted lines. The wave-packet parameters were the same as those used in Figure 10.19. The potential was $V = 0$ on the left ($x < 0.6$) and $V = 1 \times 10^6$ on the right ($x \geq 0.6$). Left: plots of $\psi^* \psi$ at various times, with time increasing as we move down the sequence. The particle initially traveled from left to right, was reflected from the wall, and then traveled toward the left. Note that the wave packet at the bottom was significantly broader than the initial packet, due to the spreading effects discussed above. Right: expanded plot of two views recorded as the wave was "striking" the wall.

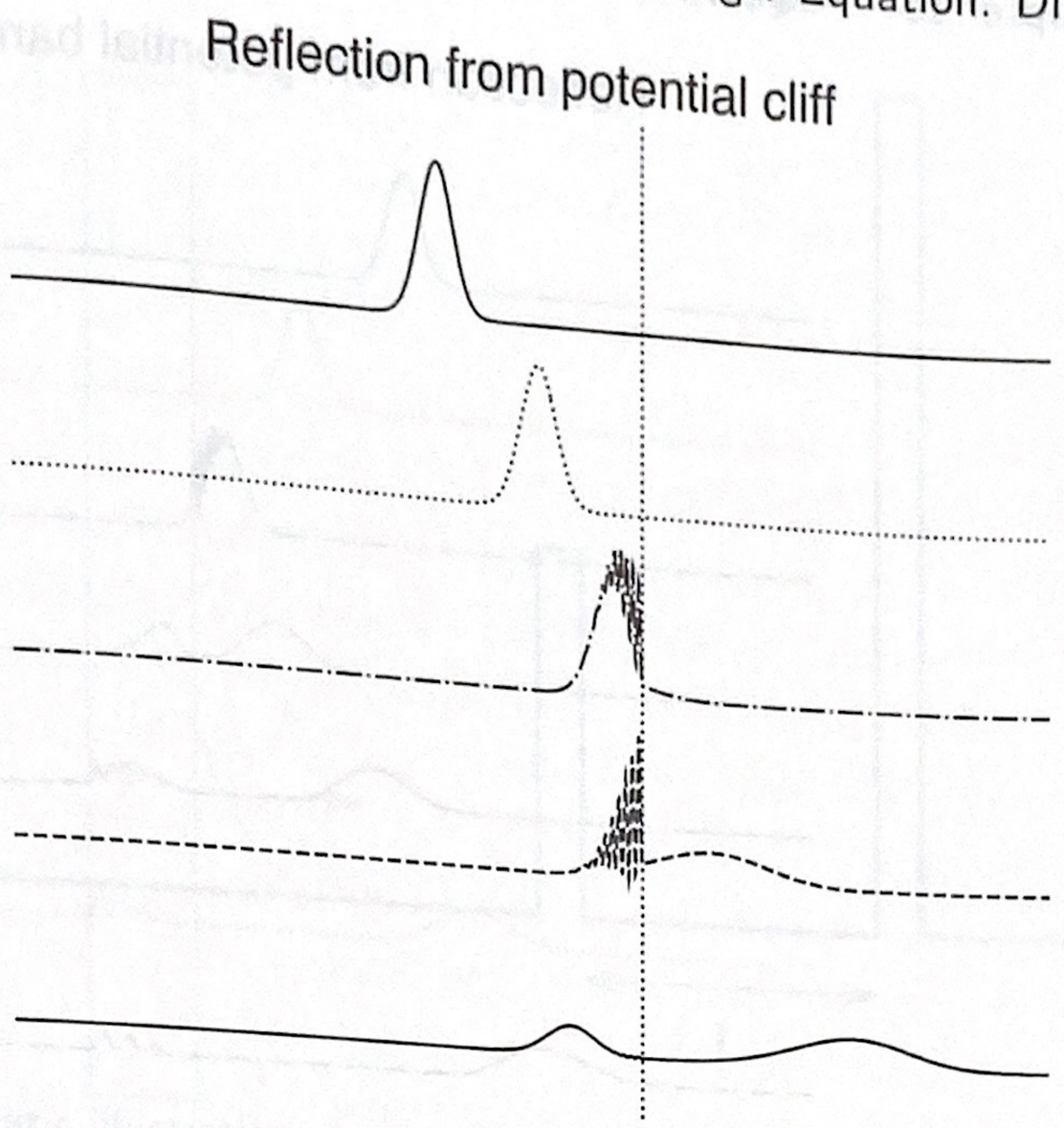

FIGURE 10.21: Wave packet incident on a cliff whose position is indicated by the vertical dotted line. The wave-packet parameters were the same as those used in Figure 10.20. The potential was $V = 0$ on the left ($x < 0.6$) and $V = -1 \times 10^6$ on the right ($x \geq 0.6$). These are plots of $\psi^*\psi$ at various times, with time increasing as we move down the graph. The particle initially traveled from left to right. After the encounter with the cliff, a small packet continued to the right, while another packet was reflected and traveled to the left. Note that the transmitted packet has a higher speed than the reflected one, since in this region the kinetic energy is higher (due to the lower potential energy).

conclude that a quantum world would be a safer place to live, since it would be harder to fall off a quantum cliff than a classical one.

As a final example in this section we consider a wave packet incident on a barrier. Here the potential was $V_0 = 1.25 \times 10^5$ in the region $0.6 \leq x \leq 0.7$, with $V = 0$ to the left and right of the barrier. We chose this value of V_0 since it was equal to the "average" kinetic energy for this wave packet, $\hbar^2 k_0^2/2m$. We see from Figure 10.22 that the incident packet was mainly reflected. If we had plotted the results on a greatly expanded scale, you would observe that a small amount was also transmitted. In addition, on the time scale considered here a small amount of the packet "remained behind" in the barrier region. The velocity in this region is essentially zero, since the average kinetic energy is $\hbar^2 k_0^2/2m - V = 0$, so it takes a long time for a wave packet in this region to escape.

The general approach to the time-dependent Schrödinger equation, which we have described in this section, can be applied to a very wide variety of problems. Further examples will be explored in the exercises.

EXERCISES

10.14. Study the motion of a propagating wave packet in free space as in Figure 10.19 and show quantitatively that it does indeed move with a velocity of $\hbar k_0/m$. Compare the behavior with different values of k_0. You should find that as k_0 is made larger, our algorithm requires smaller spatial and time steps to avoid

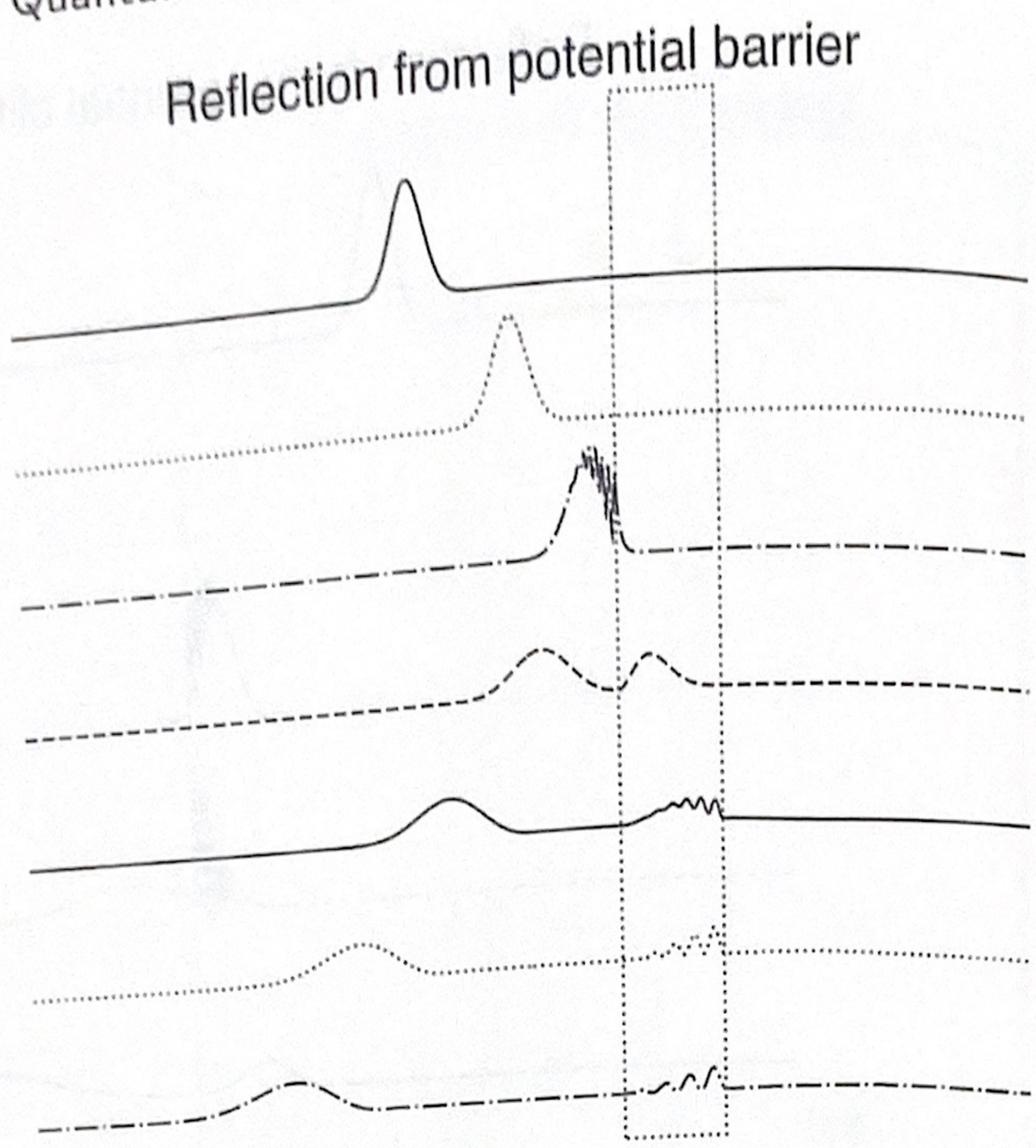

FIGURE 10.22: Wave packet partially reflecting from a potential barrier (indicated by the dotted lines) with $V = 1.25 \times 10^5$. The other parameters were the same as used in Figure 10.20. The packet initially traveled from left to right (top). Part of the packet was reflected and traveled away to the left, while a very small part (which is barely visible on the scale used here) was transmitted and proceeded to the right.

substantial numerical errors. These errors are not significant for the values of Δx and Δt we have used in the calculations in this section, but this would not have been the case if we had employed somewhat larger values of k_0.

10.15. Study how the rate of wave-packet spreading as observed in Figure 10.17 varies with the width of the initial packet. Compare this spreading quantitatively with the Heisenberg uncertainty relation. Do this by calculating the width of the wave packet as a function of time.

10.16. Observe the propagation of a wave packet in a region in which the potential increases linearly with position. Study the reflection of the wave packet in this case.

***10.17.** Study reflection and transmission from a barrier for which the potential is greater than the kinetic energy of the incident wave packet. The probability for the particle to tunnel through such a barrier decreases rapidly as the potential is increased. In order to have a significant transmission probability you will have to make the barrier thinner than in Figure 10.22. *Hint:* Good parameter choices are $k_0 = 700$, $\Delta t = 5 \times 10^{-7}$, and $\Delta x = 5 \times 10^{-4}$. Let the height of the potential barrier be $V_0 = 2 \times k_0^2$ with a width of 0.05. You should also explore the behavior for other values of both V_0 and the width of the barrier.

***10.18.** Compute the scattering of a wave packet from the potential well shown in Figure 10.23. Try to observe effects associated with the bound states in the well. *Hint:* Start with the wave-packet parameters given in the previous problem. Assuming that the particle is incident from the left, take the height of the left-most barrier to be $4k_0^2$ and give it a width of 0.05. Give the right-most barrier the same width and a much larger height, and let the two barriers be separated by $L = 1$ (or less). You should find that the penetration of the wave function into

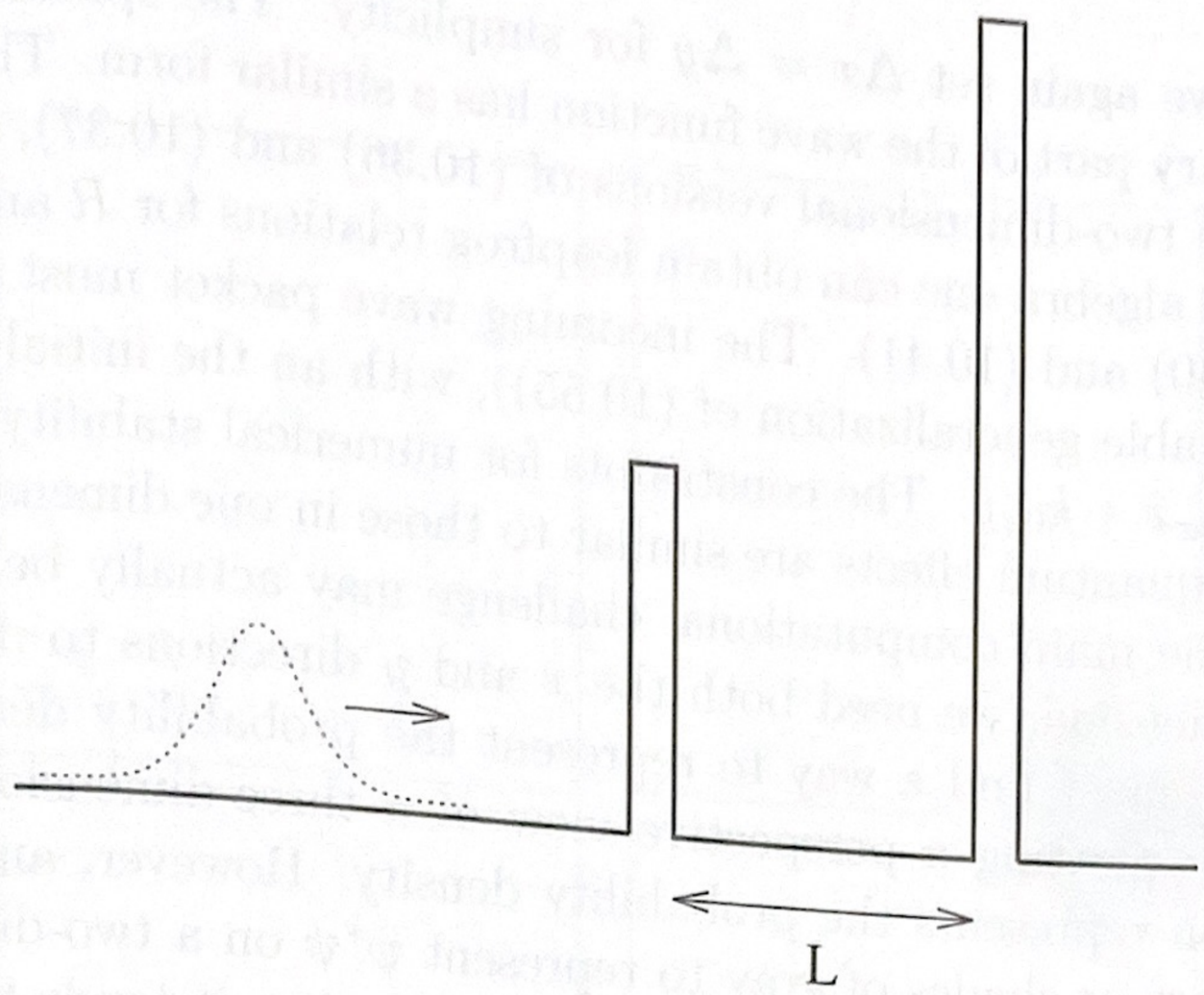

FIGURE 10.23: Schematic illustration of a wave packet (dotted curve) incident on a region containing two potential barriers. $V = 0$ on the left, on the right, and between the barriers. The barrier heights are greater than the kinetic energy of the particle.

the potential well depends on the value of k_0 and that this penetration is greatest when the energy of the particle matches the energy of one of the approximate bound states of the well.

10.6 TIME-DEPENDENT SCHRÖDINGER EQUATION IN TWO DIMENSIONS

In this section we extend the leapfrog method introduced in the previous section to two dimensions. The further extension to three dimensions is straightforward, although plotting (and making sense of!) the results becomes more difficult as the spatial dimension grows.

When working in two dimensions, our discrete versions of the potential $V(x, y)$ and the functions $\psi(x, y, t) = R(x, y, t) + \imath I(x, y, t)$ have two spatial indices, and $\psi(x, y)$ must now be normalized on a two-dimensional grid. However, the modifications required to the numerical algorithm in (10.40) and (10.41) are relatively minor. The replacement of $\partial^2/\partial x^2$ in the one-dimensional Hamiltonian (10.34) by the two-dimensional Laplacian ∇^2 changes the spatial derivative term (10.38) for the real part of ψ (the function R), and for the imaginary part of ψ (the function I). We still use centered differences to approximate these derivatives, and for the real part of the wave function we get

$$\begin{aligned}\nabla^2 R(x,y,t) &\approx \frac{R(x+\Delta x,y,t) - 2R(x,y,t) + R(x-\Delta x,y,t)}{(\Delta x)^2} \\ &\quad + \frac{R(x,y+\Delta y,t) - 2R(x,y,t) + R(x,y-\Delta y,t)}{(\Delta y)^2} \\ &= \frac{R(x+\Delta x,y,t) + R(x-\Delta x,y,t) + R(x,y+\Delta x,t) + R(x,y-\Delta y,t) - 4R(x,y,t)}{(\Delta x)^2}, \end{aligned} \tag{10.56}$$

where we again set $\Delta x = \Delta y$ for simplicity. The spatial derivative term for the imaginary part of the wave function has a similar form. These can then be inserted into the two-dimensional versions of (10.36) and (10.37), and after some straightforward algebra one can obtain leapfrog relations for R and I which are analogous to (10.40) and (10.41). The incoming wave packet must also be two dimensional (by suitable generalization of (10.55)), with an the initial wave vector of the form $\mathbf{k}_0 = k_{0x}\hat{x} + k_{0y}\hat{y}$. The constraints for numerical stability and accuracy as well as for the quantum effects are similar to those in one dimension.

The main computational challenge may actually be visualization. Unlike in one dimension, we need both the x and y directions to describe the position and thus we must find a way to represent the probability density $\psi^*\psi$. This is often done by plotting a perspective view of a three-dimensional surface where the z direction represents the probability density. However, another effective way is to use colors or shades of gray to represent $\psi^*\psi$ on a two-dimensional grid. In what follows, we will mostly use the latter method as it tends to require less computing and does not require sophisticated graphics routines.

Some typical results are shown in Figure 10.24, where the wave packet scatters from a cylindrical potential well of radius $a = 0.2$ centered at the origin of a square grid with x and y ranging from -1 to 1. The well has a depth $V_0 = -1000$, and a Gaussian wave packet of incident energy $k_0 = 800$ is incident from the left. Successive plots describe the time evolution of the wave packet from $t = 0$ through $t = 0.02$ (the time step for the calculation was $\Delta t = 0.0001$). For this case of the kinetic energy of the incoming wave packet on the same order as the depth of the potential well, and we find large oscillations in the probability amplitude near the edges of the well (as we also observed in one-dimension), and most of the packet is eventually transmitted to the right. There is also a small reflected wave, but it is hard to see in this figure because its amplitude is very small. We also find that transmission and reflection occur not just along the incoming axis but also *around* the well, and the main transmitted amplitude spreads laterally as well. In two dimensions, there are simply many more paths the wave packet can take, allowing parts of the packet to avoid going *through* the well.

Another example is shown in Figure 10.25, where the same incoming wave packet impinges on a cylindrical potential barrier instead. The incoming wave packet energy is now a bit smaller than the barrier height, so one would expect large quantum effects. Recall that in one dimension this situation typically results in significant penetration of the packet into the classically forbidden barrier interior, followed by reflection and transmission, with a small third wave portion of the wave function remaining trapped inside the barrier. The result in two dimensions is somewhat different. From Figure10.25, we see that the bulk of the incident wave packet goes *around* the barrier instead of *through* it. However, similar to one dimension, a small portion of the wave penetrates the barrier and lingers there for quite some time after the main part of the packet passes by, though this is hard to see from these figures. In order to illustrate the last point, we also show in Figure 10.26 the three-dimensional surface view at $t = 0.0250$. We clearly see a small peak right near the center of the barrier (the origin), while most of the wave packet has either gone around the barrier or been reflected.

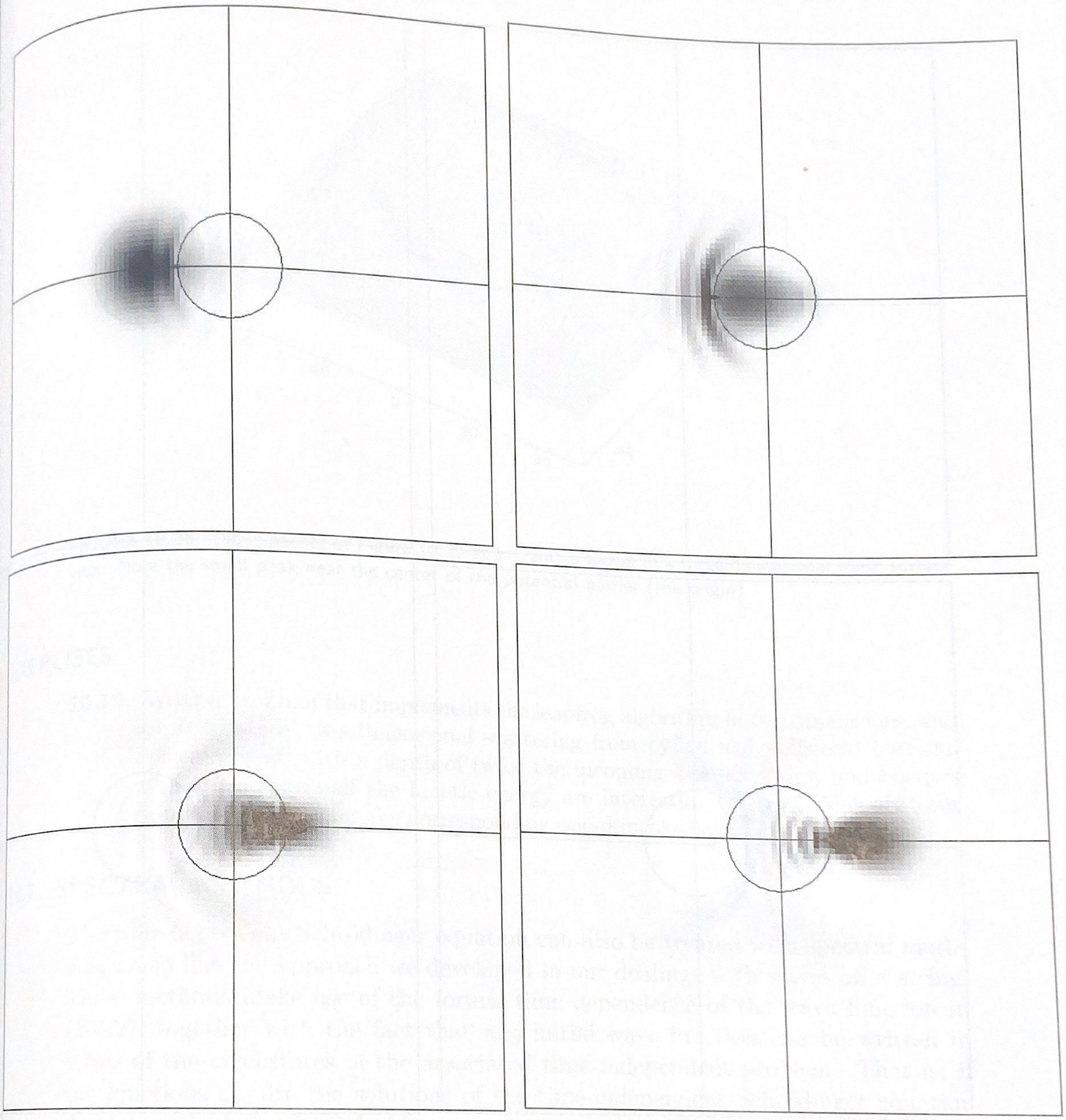

FIGURE 10.24: Wave packet of $k_0 = 40$ impinging on a well of depth $V_0 = -1000$, where $\sigma = 0.1$ and $x_0 = -0.5$. The shades of gray linearly progress toward black as the probability density rises. Shown on upper left is the probability density at $t = 50\Delta t = 0.0050$, upper right $t = 0.0100$, lower left $t = 0.0150$, and lower right $t = 0.0200$. The space is discretized in units of $\Delta x = 0.02$; x and y range between -1 and 1.

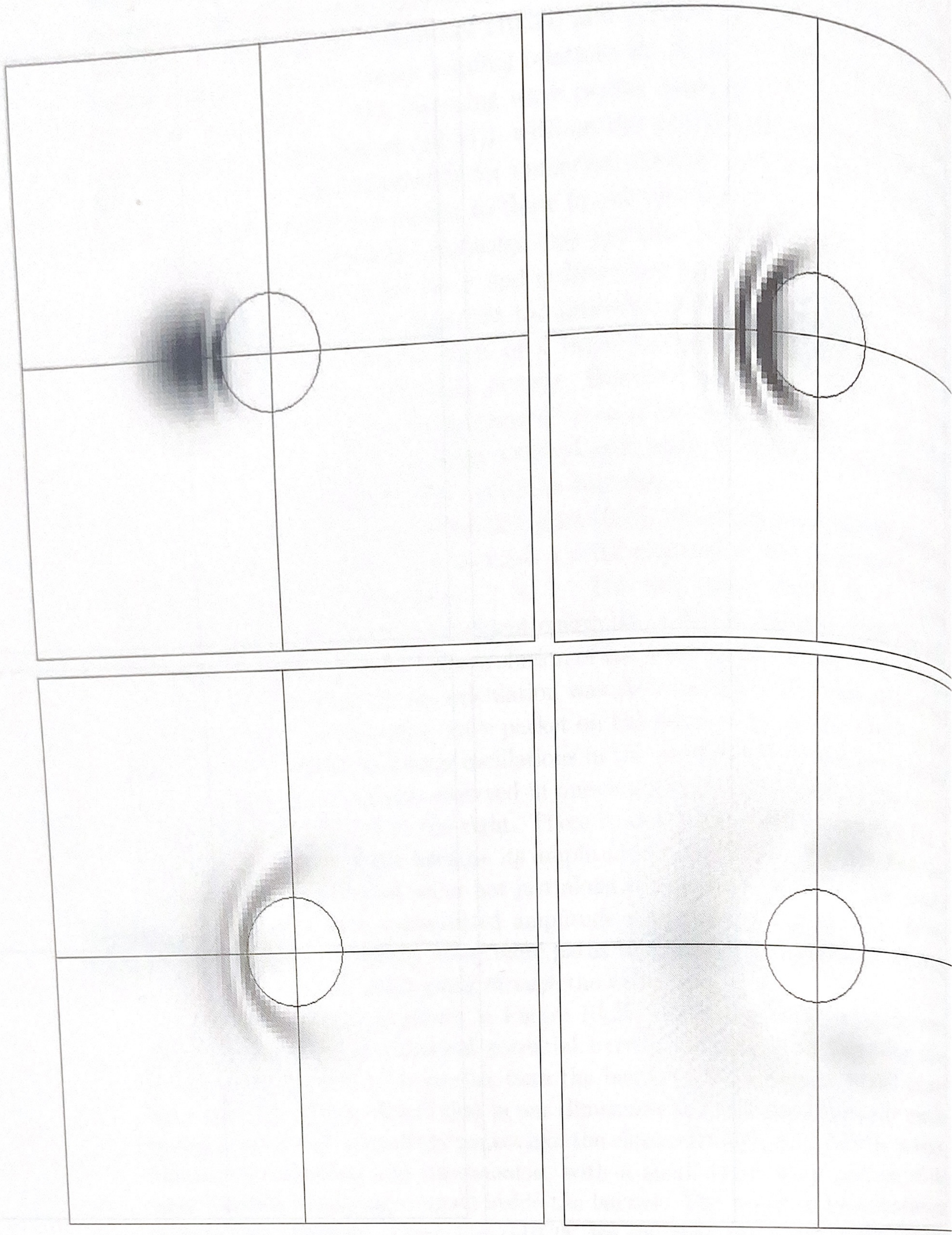

FIGURE 10.25: Wave packet with $k_0 = 40$, $\sigma = 0.1$, and $x_0 = -0.5$, impinging on a barrier of height $V_0 = 1000$. The shades of grey linearly progress toward black as the probability density rises. Shown at the upper left is the probability density at $t = 50\Delta t = 0.0050$, at $t = 0.0100$ (upper right), at $t = 0.0150$ (lower left), and $t = 0.0200$ (lower right). Space is discretized in units of $\Delta x = 0.02$, and the ranges of x and y are between -1 and 1. The time step was $\Delta t = 0.0001$.

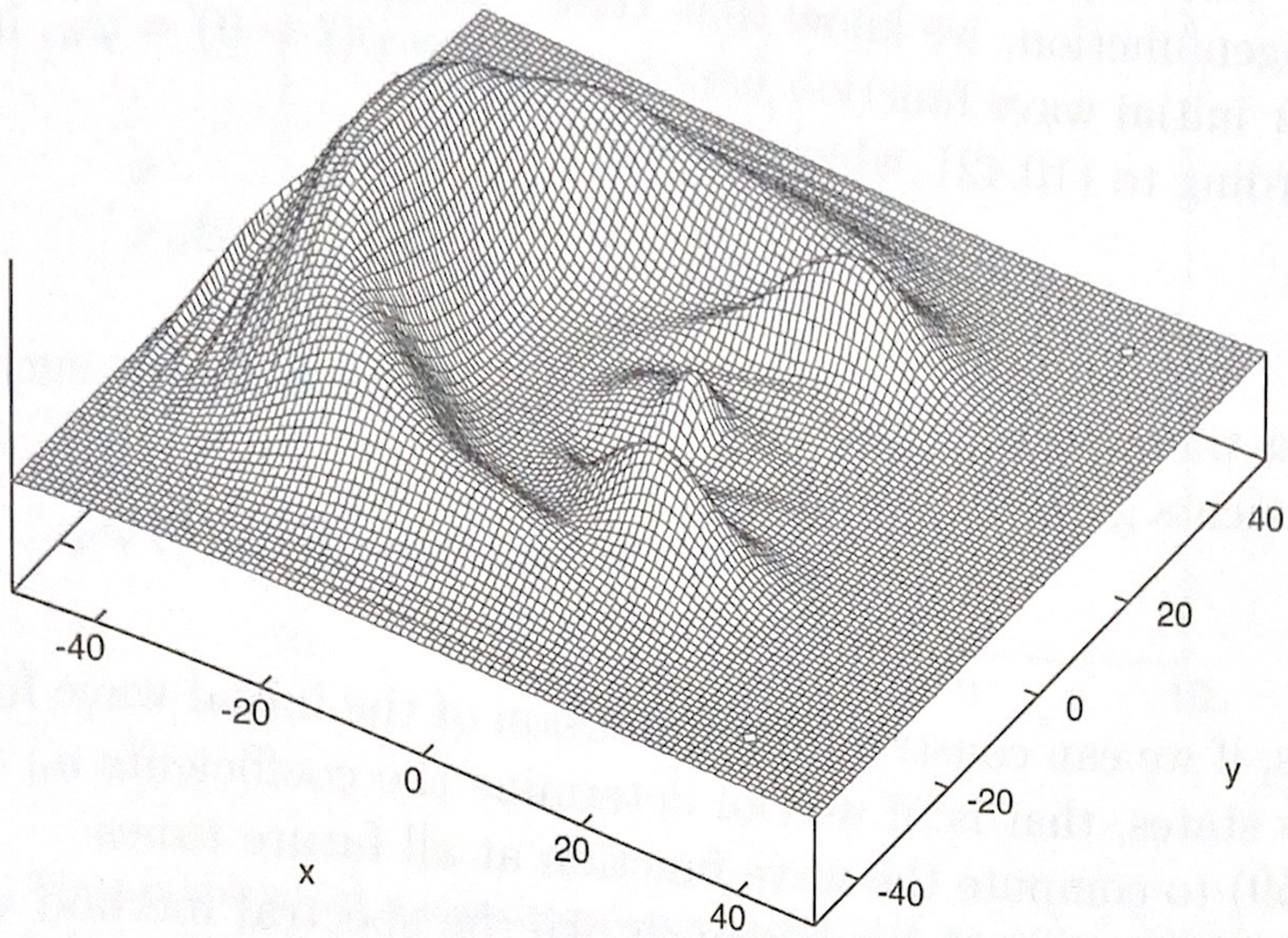

FIGURE 10.26: Wave packet of Figure 10.25 at $t = 250$ is shown in a three-dimensional mesh surface view. Note the small peak near the center of the potential barrier (the origin).

EXERCISES

10.19. Write a program that implements the leapfrog algorithm in two dimensions, and use it to study two-dimensional scattering from cylindrical wells and barriers. Potential wells with a depth of twice the incoming kinetic energy, and barriers with a height of half the kinetic energy are interesting choices. Compare your results with those for the corresponding one-dimensional problem.

10.7 SPECTRAL METHODS

The time-dependent Schrödinger equation can also be treated with spectral methods, much like the approach we developed in our dealings with waves on a string. These methods make use of the formal time dependence of the wave function in (10.42), together with the fact that *any* initial wave function can be written in terms of the eigenstates of the associated time-*in*dependent problem. That is, if the functions φ_n are the solutions of the time-independent Schrödinger equation for the particular potential of interest, any wave packet ψ can be written as

$$\psi = \sum_n a_n \varphi_n , \tag{10.57}$$

where the a_n are complex constants. Note that here the label n is used to refer to different eigenstates, that is, energy levels; it does *not* correspond to space or time. This is analogous to the Fourier expansions of arbitrary functions, which are